



Cite this: *Energy Environ. Sci.*, 2025, **18**, 3680

Industrially viable formate production with 50% lower CO₂ emissions†

Fanxu Meng,^{‡,ad} Zihan Shen,^{‡,a} Xinlong Lin,^{‡,a} Pengfei Song,^a Tianze Wu,^a Shibo Xi,^e Chao Wu,^e Zhenhui Ma,^{id f} Daniel Mandler^{id *d} and Zhichuan J. Xu^{id *abc}

The conventional production of formic acid is energy-intensive, requiring methanol and carbon monoxide reactions followed by hydrolysis under high temperature and pressure. Methanol electrochemical refinery (e-refinery) offers a sustainable alternative but faces challenges like high overpotential and competing oxygen evolution reaction (OER). This study presents Pt-nanoparticle-decorated Ni(OH)₂ as a breakthrough catalyst, achieving a significantly lower onset potential of 0.5 V vs. reversible hydrogen electrode (RHE) for methanol-to-formate conversion compared to previous reports (>1.35 V vs. RHE), while simultaneously generating hydrogen at the cathode. The platinum valence state is identified as an effective descriptor for formate faradaic efficiency, validated through experimental studies and density functional theory. Pt_{1.05}@Ni(OH)₂, featuring the highest platinum valence states among the catalysts studied, exhibits an exceptional formate faradaic efficiency of 78.8% and a high formate production rate of 1.3 mmol h⁻¹ mg_{cat}⁻¹ at 0.8 V vs. RHE. This approach reduces overpotential, eliminates OER, and cuts carbon dioxide emissions by over 50% compared to traditional methods. Moreover, economic analysis shows profitability from the fourth year at 50 mA cm⁻², supporting easier industrial adoption and low carbon dioxide emissions. These advancements offer a sustainable, energy-efficient, and economically viable method for formate production, advancing the commercialization of methanol e-refinery technology.

Received 23rd January 2025,
Accepted 5th March 2025

DOI: 10.1039/d5ee00452g

rsc.li/ees

Broader context

A transition towards sustainable chemical production has driven a great interest into alternative methods that minimize environmental impact and energy consumption. Formic acid, a versatile chemical used in various industrial applications, is traditionally produced through energy-intensive processes involving methanol and carbon monoxide reactions. Such methods contribute significantly to carbon emissions and reliance on fossil fuels. Considering the future increase in green methanol production, the greener methods to produce formic acid from methanol is desired for a significant reduction in CO₂ emission of its supply chain. Electrochemical refinery of methanol to formate meets such a need due to its high electron-to-product efficiency. However, the high overpotential and competing OER have hindered its potential for practical implementation. This paper introduces a Pt-decorated Ni(OH)₂ catalyst that significantly achieves efficient and low-overpotential formate production with co-generation of hydrogen. It covers detailed studies on how the technique overcomes key technical barriers as well as the analysis of its economic and environmental benefits. The work marks a critical step toward the large-scale adoption of methanol e-refinery technology and its integration into a low-carbon economy.

^a School of Material Science and Engineering, Nanyang Technological University, 50 Nanyang Avenue, Singapore 639798, Singapore. E-mail: xuzc@ntu.edu.sg

^b Energy Research Institute@Nanyang Technological University, ERI@N, Interdisciplinary Graduate School, Nanyang Technological University, 50 Nanyang Avenue, Singapore 639798, Singapore

^c Center for Advanced Catalysis Science and Technology, Nanyang Technological University, 50 Nanyang Avenue, Singapore, 639798, Singapore

^d Institute of Chemistry, The Hebrew University of Jerusalem, Jerusalem 9190401, Israel

^e Institute of Sustainability for Chemicals, Energy, and Environment (ISCE2), Agency for Science, Technology and Research (A*STAR), 1 Pesek Road, Jurong Island, Singapore 627833, Singapore

^f Department of Physics, Beijing Technology and Business University, Beijing 100048, China

† Electronic supplementary information (ESI) available. See DOI: <https://doi.org/10.1039/d5ee00452g>

‡ These authors contributed equally to this work.



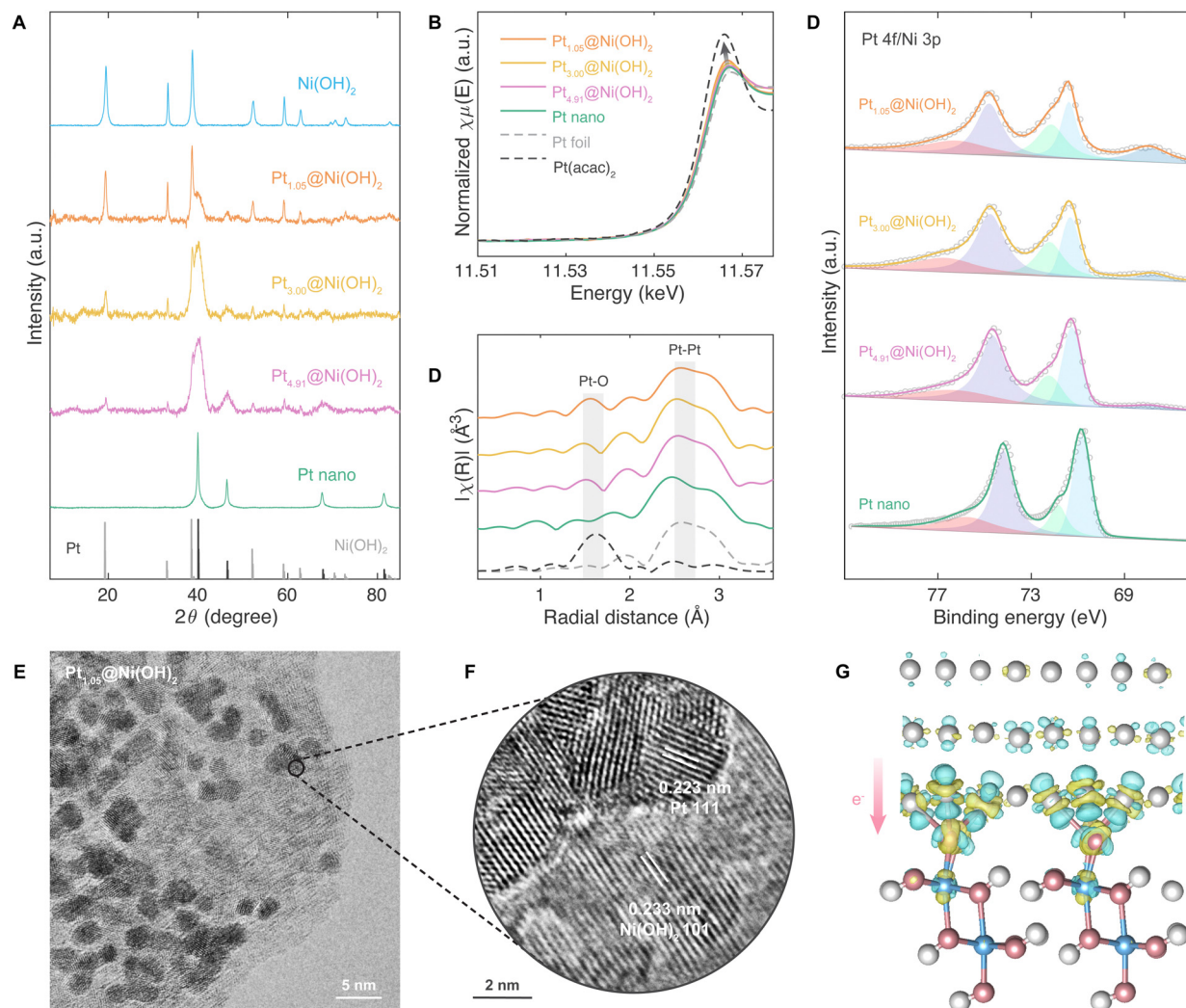


Fig. 1 Characterizations of $\text{Pt}_x\text{@Ni(OH)}_2$ ($x = 0.00, 1.05, 3.00, \text{ and } 4.91$) and Pt nano. (a) XRD, (b) XANES, (c) EXAFS, and (d) XPS spectra for $\text{Pt}_x\text{@Ni(OH)}_2$ ($x = 0.00, 1.05, 3.00, \text{ and } 4.91$) and Pt nano. (e) and (f) HRTEM images of $\text{Pt}_{1.05}\text{@Ni(OH)}_2$. (g) Charge density difference of Pt–Ni(OH)₂ heterojunction. The cyan regions indicate charge depletion, while the yellow regions represent charge accumulation, with an isosurface value of $0.01 \text{ e } \text{Å}^{-3}$.

observed in the HRTEM figures in Fig. 1f and Fig. S4 (ESI[†]). Self-consistent calculations have confirmed the charge-deficient status of the Pt layer, thereby validating the experimental findings from a theoretical perspective.

Methanol e-refinery performance

To assess the performance of $\text{Pt}_x\text{@Ni(OH)}_2$ and Pt nano in methanol e-refinery processes, cyclic voltammetry (CV) and chronoamperometry (CA) experiments at 0.8 V vs. RHE are conducted using the five electrocatalysts in a typical H-type electrochemical cell. The cell comprises distinct anode and cathode compartments. In the cathodic chamber, a platinum plate ($1 \times 2 \text{ cm}^2$) functions as the counter electrode, facilitating the hydrogen evolution reaction (HER). Within the anodic chamber, a Hg/HgO electrode serves as the reference electrode, while a catalyst-modified glassy carbon electrode acts as the working electrode, where the electrochemical conversion of methanol takes place. Following electrochemical testing, nuclear magnetic resonance

(NMR) and ion chromatography (IC), analyses are carried out to identify potential reaction products. Fig. 2a displays the CV curves for each electrocatalyst, revealing that an increase in Pt content is accompanied by a corresponding increase in the methanol oxidation peak for $\text{Pt}_x\text{@Ni(OH)}_2$ ($x = 0.00, 1.05, 3.00, \text{ and } 4.91$). A representative CA profile for $\text{Pt}_{1.05}\text{@Ni(OH)}_2$ is presented in Fig. S5 (ESI[†]). In Fig. 2b, NMR spectra for the five catalysts show a gradual increase in the peak⁵⁸ corresponding to HCOO^- as the catalyst transitions from Ni(OH)_2 to $\text{Pt}_{4.91}\text{@Ni(OH)}_2$. HCHO , located around 4.4 ppm ,⁵⁹ is not observed, indicating its absence in the methanol e-refinery products. Fig. 2c presents the IC curves for Pt nano, with peaks at 2.9 min and 4.6 min attributed to HCOO^- and CO_3^{2-} , respectively, suggesting the production of abundant HCOO^- and CO_3^{2-} on Pt nano.

Fig. 3a and b provide a summary of the formate production rate and faradaic efficiency after 2-hour CA test at 0.8 V vs. RHE . Two notable observations emerge from these figures. Firstly, Ni(OH)_2 fails to activate methanol at 0.8 V vs. RHE . Secondly,





Fig. 2 Electrochemical performances of $\text{Pt}_x\text{@Ni(OH)}_2$ ($x = 0.00, 1.05, 3.00,$ and 4.91) and Pt nano. (a) CV profiles in 1 M KOH + 1 M CH_3OH in comparison with 1 M KOH on $\text{Pt}_x\text{@Ni(OH)}_2$ ($x = 0.00, 1.05, 3.00,$ and 4.91) and Pt nano. (b) NMR spectra of the five catalysts. The positions for HCOO^- and HCHO are around 8.3 ppm and 4.4 ppm,^{58,59} respectively. No peaks for HCHO are observed for all catalysts. (c) IC patterns of Pt nano. To counteract CO_2 adsorption from open air, IC tests are conducted before and after the CA experiments.

the formate production rate increases with the Pt ratio on $\text{Pt}_x\text{@Ni(OH)}_2$ ($x = 1.05, 3.00,$ and 4.91), albeit with a gradual decrease in faradaic efficiency. The first observation aligns with the CV curves depicted in Fig. 2a, indicating Ni(OH)_2 's incapacity to convert methanol at 0.8 V vs. RHE. The slight enhancement in formate production rate in the second observation results from the increase in Pt content among $\text{Pt}_x\text{@Ni(OH)}_2$ ($x = 1.05, 3.00,$ and 4.91). In contrast, the variation in formate faradaic efficiency is attributed to the heightened valence states

of $\text{Pt}_x\text{@Ni(OH)}_2$ ($x = 1.05, 3.00,$ and 4.91), as evidenced by the X-ray absorption spectroscopy (XAS) and XPS curves presented in Fig. 1b–d, indicating its potential capability as an efficient descriptor for methanol-to-formate faradaic efficiencies. Additionally, Fig. 3c compares the onset potential and formate faradaic efficiency of $\text{Pt}_{1.05}\text{@Ni(OH)}_2$ with other methanol e-refinery catalysts reported in the literature, highlighting the significantly lower operation potential of $\text{Pt}_{1.05}\text{@Ni(OH)}_2$ compared to previous findings.^{17–21}



Fig. 3 Methanol e-refinery product analysis of $\text{Pt}_x\text{@Ni(OH)}_2$ ($x = 0.00, 1.05, 3.00,$ and 4.91) and Pt nano. (a) Formate production rate and (b) faradaic efficiency. (c) Performance comparison between $\text{Pt}_{1.05}\text{@Ni(OH)}_2$ and other methanol e-refinery catalysts in the literature.



Methanol e-refinery mechanisms

Fig. 4a clearly illustrates the direct relationship between formate faradaic efficiency and the Pt $4f_{5/2}$ energy, which is an indicator of Pt valence states, showing a near-linear relationship. Similarly, Fig. S6a and c (ESI[†]) depicts the relationships between formate faradaic efficiency and both the Pt $4f_{7/2}$ binding energy and the white-line intensity in XANES analysis, respectively, both of which display comparable proportional dependencies. Fig. 4b systematically illustrates this phenomenon. Furthermore, the energy variations of the methanol e-refinery reaction on Pt-loaded Ni(OH)₂ and pure Pt nanoparticles are calculated to better illustrate the correlation between Pt valence states and formate faradaic efficiency. The reaction route follows previous literature reports:^{45,48–52,60} the first three steps are methanol deprotonation processes, forming a *CHO intermediate, followed by two hydroxide-attacking steps to produce HCOO[−] (refer to Fig. 4c). The energy profiles of Pt@Ni(OH)₂ compared to pristine Pt nanoparticles have also been delineated in Fig. 4c. Notably, the Pt@Ni(OH)₂ demonstrates a diminished energy barrier for the rate-limiting step, corroborating the beneficial influence of the elevated valence state of platinum on the catalytic conversion of methanol to formate.

Moreover, to further substantiate the relationship between Pt valence states and formate production from methanol, a 5-minute methanol e-refinery reaction at 0.8 V vs. RHE is conducted on Pt_{1.05}@Ni(OH)₂ following a 5-minute HER in

1 M KOH at −0.1 V vs. RHE. This process is repeated 24 times successively, resulting in a total methanol e-refinery time of 2 hours. The formate faradaic efficiency exhibits a decrease to approximately 60.0% (Fig. S7, ESI[†]) compared to that of Pt_{1.05}@Ni(OH)₂ in Fig. 3b, thus reinforcing the correlation between Pt valence states and formate faradaic efficiency. Additionally, the formate faradaic efficiency is examined for Pt nanoparticles loaded on Co(OH)₂ under identical CA conditions, as shown in Fig. S8 (ESI[†]). Pt@Co(OH)₂ demonstrates a noteworthy formate faradaic efficiency of approximately 77.0%. The results from both experiments provide further evidence supporting the wide applicability and effectiveness of the Pt-valence-state descriptor for the methanol e-refinery process.

MEA membrane electrode assembly test

Leveraging the promising properties of Pt_{1.05}@Ni(OH)₂, this anode is incorporated into a 2 × 2 cm² membrane electrode assembly (MEA) cell configuration, as detailed in a prior study.²⁰ The MEA cell, schematically represented in Fig. 5a, features an anion exchange membrane (AEM) that segregates the cathode and anode compartments. In this setup, Pt_{1.05}@Ni(OH)₂ (2 mg cm^{−2}) serves as the anode catalyst, while commercial Pt/C (1 mg cm^{−2}) is employed as the cathode catalyst.

To assess the electrochemical performance of the catalyst, polarization results are generated by performing a 3-minute



Fig. 4 Methanol e-refinery mechanisms towards formate. (a) The relationship between Pt $4f_{5/2}$ energy and formate faradaic efficiencies of Pt_x@Ni(OH)₂ ($x = 1.05, 3.00,$ and 4.91) and Pt nano. (b) The reaction diagram of methanol e-refinery on Pt-loaded Ni(OH)₂. (c) Possible reaction route and the corresponding computed free energy changes of methanol e-refinery towards formate on Pt and Pt-loaded Ni(OH)₂.





Fig. 5 MEA test on Pt_{1.05}@Ni(OH)₂. (a) Schematic diagram for the methanol e-refinery MEA cell. (b) HCOO⁻ production rates and faradaic efficiencies at 10, 20, 30, 40, and 50 mA cm⁻² in 1 M KOH + 1 M CH₃OH. (c) Comparative analysis of global warming impacts for the methanol e-refinery MEA cell vs. industrial formic acid production at 10, 20, 30, 40, and 50 mA cm⁻². (d) Detailed environmental impact assessment of the methanol e-refinery MEA cell compared to industrial formic acid production. (e) Cost analysis for the methanol e-refinery MEA cell. (f) Comparative evaluation of production costs for the methanol e-refinery MEA cell vs. the commercial formic acid price. (g) Cumulative net profit analysis for the methanol e-refinery MEA cell plant.

chronopotentiometry (CP) test for both 1 M KOH + 1 M CH₃OH and 1 M KOH electrolytes at current densities of 10, 20, 30, 40, and 50 mA cm⁻² (geometric area), a temperature of 80 °C, and an electrolyte flow rate of 2 ml min⁻¹. Notably, the methanol e-refinery reaction exhibited a considerably lower potential compared to OER on Pt_{1.05}@Ni(OH)₂ at a fixed current density, as depicted in Fig. S9a (ESI[†]).

Following the polarization experiments, a 30-minute CP test is conducted at current densities of 10, 20, 30, 40, and 50 mA cm⁻² (geometric area) in 1 M KOH + 1 M CH₃OH, as presented in Fig. S9b (ESI[†]). The electrolytes are subsequently analyzed by IC to quantify the concentration of formate ions (HCOO⁻). Fig. 5b illustrates the production rate and faradaic efficiency of HCOO⁻. Notably, formate faradaic efficiency takes a considerable share at all current densities.



References

- W. F. Lamb, T. Wiedmann, J. Pongratz, R. Andrew, M. Crippa, J. G. J. Olivier, D. Wiedenhofer, G. Mattioli, A. A. Khourdajie, J. House, S. Pachauri, M. Figueroa, Y. Saheb, R. Slade, K. Hubacek, L. Sun, S. K. Ribeiro, S. Khennas, S. de la Rue du Can, L. Chapungu, S. J. Davis, I. Bashmakov, H. Dai, S. Dhakal, X. Tan, Y. Geng, B. Gu and J. Minx, *Environ. Res. Lett.*, 2021, **16**, 073005.
- P. De Luna, C. Hahn, D. Higgins, S. A. Jaffer, T. F. Jaramillo and E. H. Sargent, *Science*, 2019, **364**, eaav3506.
- S. Mou, T. Wu, J. Xie, Y. Zhang, L. Ji, H. Huang, T. Wang, Y. Luo, X. Xiong, B. Tang and X. Sun, *Adv. Mater.*, 2019, **31**, 1903499.
- L. Ji, L. Li, X. Ji, Y. Zhang, S. Mou, T. Wu, Q. Liu, B. Li, X. Zhu, Y. Luo, X. Shi, A. M. Asiri and X. Sun, *Angew. Chem., Int. Ed.*, 2020, **59**, 758–762.
- T. Ahmad, S. Liu, M. Sajid, K. Li, M. Ali, L. Liu and W. Chen, *Nano Res. Energy*, 2022, **1**, 9120021.
- L. Li, I. M. U. Hasan, Farwa, R. He, L. Peng, N. Xu, N. K. Niazi, J.-N. Zhang and J. Qiao, *Nano Res. Energy*, 2022, **1**, 9120015.
- B. S. Crandall, B. H. Ko, S. Overa, L. Cherniack, A. Lee, I. Minnie and F. Jiao, *Nat. Chem. Eng.*, 2024, **1**, 421–429.
- J. Lee, S. M. Kim, B. W. Jeon, H. W. Hwang, E. G. Poloniataki, J. Kang, S. Lee, H. W. Ra, J. Na, J.-G. Na, J. Lee and Y. H. Kim, *Nat. Chem. Eng.*, 2024, **1**, 354–364.
- Z. Li, P. Wang, X. Lyu, V. K. R. Kondapalli, S. Xiang, J. D. Jimenez, L. Ma, T. Ito, T. Zhang, J. Raj, Y. Fang, Y. Bai, J. Li, A. Serov, V. Shanov, A. I. Frenkel, S. D. Senanayake, S. Yang, T. P. Senftle and J. Wu, *Nat. Chem. Eng.*, 2024, **1**, 159–169.
- J. E. Huang, Y. Chen, P. Ou, X. Ding, Y. Yan, R. Dorakhan, Y. Lum, X.-Y. Li, Y. Bai, C. Wu, M. Fan, M. G. Lee, R. K. Miao, Y. Liu, C. O'Brien, J. Zhang, C. Tian, Y. Liang, Y. Xu, M. Luo, D. Sinton and E. H. Sargent, *J. Am. Chem. Soc.*, 2024, **146**, 8641–8649.
- E. Shirzadi, Q. Jin, A. S. Zeraati, R. Dorakhan, T. J. Goncalves, J. Abed, B.-H. Lee, A. S. Rasouli, J. Wicks, J. Zhang, P. Ou, V. Boureau, S. Park, W. Ni, G. Lee, C. Tian, D. M. Meira, D. Sinton, S. Siahrostami and E. H. Sargent, *Nat. Commun.*, 2024, **15**, 2995.
- X. Wang, Y. Chen, F. Li, R. K. Miao, J. E. Huang, Z. Zhao, X.-Y. Li, R. Dorakhan, S. Chu, J. Wu, S. Zheng, W. Ni, D. Kim, S. Park, Y. Liang, A. Ozden, P. Ou, Y. Hou, D. Sinton and E. H. Sargent, *Nat. Commun.*, 2024, **15**, 616.
- X. Wang, P. Li, J. Tam, J. Y. Howe, C. P. O'Brien, A. Sedighian Rasouli, R. K. Miao, Y. Liu, A. Ozden, K. Xie, J. Wu, D. Sinton and E. H. Sargent, *Nat. Sustainability*, 2024, **7**, 931–937.
- Y. Liang, F. Li, R. K. Miao, S. Hu, W. Ni, S. Zhang, Y. Liu, Y. Bai, H. Wan, P. Ou, X.-Y. Li, N. Wang, S. Park, F. Li, J. Zeng, D. Sinton and E. H. Sargent, *Nat. Synth.*, 2024, **3**, 1104–1112.
- J. Ott, V. Gronemann, F. Pontzen, E. Fiedler, G. Grossmann, D. B. Kersebohm, G. Weiss and C. Witte, *Methanol, Ullmann's Encyclopedia of Industrial Chemistry*, Wiley-VCH, Weinheim, Germany, 2012.
- P. Gautam, Neha, S. N. Upadhyay and S. K. Dubey, *Fuel*, 2020, **273**, 117783.
- M. Li, X. Deng, K. Xiang, Y. Liang, B. Zhao, J. Hao, J. L. Luo and X. Z. Fu, *ChemSusChem*, 2020, **13**, 914–921.
- K. Xiang, D. Wu, X. Deng, M. Li, S. Chen, P. Hao, X. Guo, J. L. Luo and X. Z. Fu, *Adv. Funct. Mater.*, 2020, **30**, 1909610.
- J. Li, C. Xing, Y. Zhang, T. Zhang, M. C. Spadaro, Q. Wu, Y. Yi, S. He, J. Llorca, J. Arbiol, A. Cabot and C. Cui, *Small*, 2021, **17**, e2006623.
- F. Meng, C. Dai, Z. Liu, S. Luo, J. Ge, Y. Duan, G. Chen, C. Wei, R. R. Chen, J. Wang, D. Mandler and Z. J. Xu, *eScience*, 2022, **2**(1), 87–94.
- J. Hao, J. Liu, D. Wu, M. Chen, Y. Liang, Q. Wang, L. Wang, X.-Z. Fu and J.-L. Luo, *Appl. Catal., B*, 2021, **281**, 119510.
- Z. Pi and H. Zhong, *IOP Conf. Ser. Earth Environ. Sci.*, 2021, **651**, 042062.
- M. I. Abdullah, A. Hameed, N. Zhang, M. H. Islam, M. Ma and B. G. Pollet, *ACS Appl. Mater. Interfaces*, 2021, **13**, 30603–30613.
- A. A. Dubale, Y. Zheng, H. Wang, R. Hübner, Y. Li, J. Yang, J. Zhang, N. K. Sethi, L. He, Z. Zheng and W. Liu, *Angew. Chem., Int. Ed.*, 2020, **59**, 13891–13899.
- S.-N. Sun, L.-Z. Dong, J.-R. Li, J.-W. Shi, J. Liu, Y.-R. Wang, Q. Huang and Y.-Q. Lan, *Angew. Chem., Int. Ed.*, 2022, **61**, e202207282.
- Y. Fan, X. Yang, E. Wei, Y. Dong, H. Gao, X. Luo and W. Yang, *Appl. Catal., B*, 2024, **345**, 123716.
- Y. Xu, M. Liu, M. Wang, T. Ren, K. Ren, Z. Wang, X. Li, L. Wang and H. Wang, *Appl. Catal., B*, 2022, **300**, 120753.
- B. Neppolian, *Ceram. Int.*, 2022, **48**, 29025–29030.
- J. Chen, M. Ahmad, Y. Zhang, H. Ye, L. Wang, J. Zhang, X.-Z. Fu and J.-L. Luo, *J. Chem. Eng.*, 2023, **454**, 140056.
- Y. Hao, D. Yu, S. Zhu, C.-H. Kuo, Y.-M. Chang, L. Wang, H.-Y. Chen, M. Shao and S. Peng, *Energy Environ. Sci.*, 2023, **16**, 1100–1110.
- Y. Lin, Y.-g Wang, X. Li, J. Zhao, H. Liu, C. Wu, L. Yang, G. Li, Z. Qi, L. Shan, Y. Jiang and L. Song, *Small*, 2024, **20**, 2311452.
- Y. Tong, X. Yan, J. Liang and S. X. Dou, *Small*, 2021, **17**, 1904126.
- Y. Qi, Y. Zhang, L. Yang, Y. Zhao, Y. Zhu, H. Jiang and C. Li, *Nat. Commun.*, 2022, **13**, 4602.
- B. Zhu, B. Dong, F. Wang, Q. Yang, Y. He, C. Zhang, P. Jin and L. Feng, *Nat. Commun.*, 2023, **14**, 1686.
- N. T. R. Kumar, S. Kamalakannan, M. Prakash, B. Viswanathan and B. Neppolian, *ACS Appl. Energy Mater.*, 2022, **5**, 2104–2111.
- Z. Li, Y. Gao, X. Meng, B. Sun, K. Song, Z. Wang, Y. Liu, Z. Zheng, P. Wang, Y. Dai, H. Cheng and B. Huang, *Cell Rep.*, 2022, **3**, 100972.
- J. Zhang, Y. Hua, H. Li, X. Zhang, C. Shi, Y. Li, L. Di and Z. Wang, *J. Chem. Eng.*, 2023, **478**, 147288.
- L. Zhao, Q. Sun, M. Li, Y. Zhong, P. Shen, Y. Lin and K. Xu, *Sci. China Mater.*, 2023, **66**, 1820–1828.
- M. Khan, M. I. Abdullah, A. Samad, Z. Shao, T. Mushiana, A. Akhtar, A. Hameed, N. Zhang, U. Schwingenschlögl and M. Ma, *Small*, 2023, **19**, 2205499.



- 40 F. Meng, Q. Wu, K. Elouarzaki, S. Luo, Y. Sun, C. Dai, S. Xi, Y. Chen, X. Lin, M. Fang, X. Wang, D. Mandler and Z. J. Xu, *Sci. Adv.*, 2023, **9**, eadh9487.
- 41 Q. Yang, C. Zhang, B. Dong, Y. Cui, F. Wang, J. Cai, P. Jin and L. Feng, *Appl. Catal., B*, 2021, **296**, 120359.
- 42 Y. Liu, S. F. Zhao, S. X. Guo, A. M. Bond, J. Zhang, G. Zhu, C. L. Hill and Y. V. Geletii, *J. Am. Chem. Soc.*, 2016, **138**, 2617–2628.
- 43 S. G. Bratsch, *J. Phys. Chem. Ref. Data*, 1989, **18**, 1–21.
- 44 S. C. S. Lai, N. P. Lebedeva, T. H. M. Housmans and M. T. M. Koper, *Top. Catal.*, 2007, **46**, 320–333.
- 45 H. A. Gasteiger, N. Markovic, P. N. Ross and E. J. Cairns, *J. Phys. Chem.*, 1993, **97**, 12020–12029.
- 46 D. Y. Chung, K.-J. Lee and Y.-E. Sung, *J. Phys. Chem. C*, 2016, **120**, 9028–9035.
- 47 S. S. Mahapatra and J. Datta, *Int. J. Electrochem.*, 2011, **2011**, 1–16.
- 48 A. Yuda, A. Ashok and A. Kumar, *Catal. Rev.*, 2020, 1–103, DOI: [10.1080/01614940.2020.1802811](https://doi.org/10.1080/01614940.2020.1802811).
- 49 Y.-W. Zhou, Y.-F. Chen, K. Jiang, Z. Liu, Z.-J. Mao, W.-Y. Zhang, W.-F. Lin and W.-B. Cai, *Appl. Catal., B*, 2021, **280**, 119393.
- 50 J.-T. Li, Q.-S. Chen and S.-G. Sun, *Electrochim. Acta*, 2007, **52**, 5725–5732.
- 51 S. X. Liu, L. W. Liao, Q. Tao, Y. X. Chen and S. Ye, *Phys. Chem. Chem. Phys.*, 2011, **13**, 9725–9735.
- 52 I. Tkach, A. Panchenko, T. Kaz, V. Gogel, K. A. Friedrich and E. Roduner, *Phys. Chem. Chem. Phys.*, 2004, **6**, 5419–5426.
- 53 C. Wei, R. R. Rao, J. Peng, B. Huang, I. E. L. Stephens, M. Risch, Z. J. Xu and Y. Shao-Horn, *Adv. Mater.*, 2019, **31**, e1806296.
- 54 D. Xiong, W. Li and L. Liu, *Chem. – Asian J.*, 2017, **12**, 543–551.
- 55 H. Jiang, Y. Guo, T. Wang, P.-L. Zhu, S. Yu, Y. Yu, X.-Z. Fu, R. Sun and C.-P. Wong, *RSC Adv.*, 2015, **5**, 12931–12936.
- 56 H. Hu, F. Xie, Y. Pei, M. Qiao, S. Yan, H. He, K. Fan, H. Li, B. Zong and X. Zhang, *J. Catal.*, 2006, **237**, 143–151.
- 57 M. A. Matin, E. Lee, H. Kim, W.-S. Yoon and Y.-U. Kwon, *J. Mater. Chem. A*, 2015, **3**, 17154–17164.
- 58 N. R. Babij, E. O. McCusker, G. T. Whiteker, B. Canturk, N. Choy, L. C. Creemer, C. V. D. Amicis, N. M. Hewlett, P. L. Johnson, J. A. Knobelsdorf, F. Li, B. A. Lorsbach, B. M. Nugent, S. J. Ryan, M. R. Smith and Q. Yang, *Org. Process Res. Dev.*, 2016, **20**, 661–667.
- 59 T. Chatterjee, E. Boutin and M. Robert, *Dalton Trans.*, 2020, **49**, 4257–4265.
- 60 T. H. M. Housmans, A. H. Wonders and M. T. M. Koper, *J. Phys. Chem. B*, 2006, **110**, 10021–10031.
- 61 A. Wibowo, N. Chiarasumran, A. Thanapimmetha, M. Saisriyoot, P. Srinophakun, N. Suriyachai and V. Champreda, *Catalysts*, 2022, **12**, 1215.
- 62 Y. Ahn, J. Byun, D. Kim, B.-S. Kim, C.-S. Lee and J. Han, *Green Chem.*, 2019, **21**, 3442–3455.
- 63 International Organization for Standardization. Environmental management: life cycle assessment; requirements and guidelines (2005).
- 64 International Organization for Standardization. ISO 14040-environmental management-life cycle assessment-principles and framework (2006).
- 65 H. Shin, K. U. Hansen and F. Jiao, *Nat. Sustainability*, 2021, **4**, 911–919.
- 66 T. R. D. Steward and J. Zuboy, *H2A central production model, version 3 user guide*, National Renewable Energy Laboratory, 2012.
- 67 M. Jouny, W. Luc and F. Jiao, *Ind. Eng. Chem. Res.*, 2018, **57**, 2165–2177.
- 68 A. Al-Qahtani, B. Parkinson, K. Hellgardt, N. Shah and G. Guillen-Gosalbez, *Appl. Energy*, 2021, **281**, 115958.
- 69 Alibaba product search: methanol 99%, category: alcohol & hydroxybenzene & ether, min order: 12 metric tons, https://www.alibaba.com/trade/search?fsb=y&IndexArea=product_en&CategoryId=&SearchText=methanol_85%2525, (accessed 2023).
- 70 Alibaba product search: formic acid 85%, category: organic acid, min order: 10 metric tons, https://www.alibaba.com/products/formic_acid_85%2525.html, (accessed 2023).
- 71 Today in energy (U.S. Energy Information Administration), <https://www.eia.gov/todayinenergy/prices.php>, (accessed 2023).

